Journal of Alloys and Compounds 480 (2009) 596–602

Contents lists available at ScienceDirect

Journal of Alloys and Compounds

journal homepage: www.elsevier.com/locate/jallcom

Study of ac impedance spectroscopy of Al doped $MnFe_{2-2x}Al_{2x}O_4$

Khalid Mujasam Batoo[a,*], Shalendra Kumar[b], Chan Gyan Lee[b], Alimuddin[a]

[a] Department of Applied Physics, Aligarh Muslim University, Aligarh 202002, India
[b] School of Nano and Advanced Materials Engineering, Changwon National University, Changwon, South Korea

ARTICLE INFO

Article history:
Received 30 September 2008
Received in revised form 30 January 2009
Accepted 30 January 2009
Available online 10 February 2009

PACS:
75.50.Gg
74.25.Nf

Keywords:
Ferrites
Impedance spectroscopy

ABSTRACT

We have reported electrical properties of Al doped $MnFe_2O_4$ ferrite using ac impedance spectroscopy as a function of frequency (42 Hz to 5 MHz) at different temperatures (300–473 K). XRD analysis shows that all the compositions are single phase cubic spinel in structure. The complex impedance analysis has been used to separate the grain and grain boundary resistance of $MnFe_{2-2x}Al_{2x}O_4$. From the analysis of impedance spectra it is found that the real (Z'), and imaginary (Z'') part of the impedance decrease with increasing frequency and both are found to decrease with Al doping up to 20%, and thereafter, these increase with further increasing the Al concentration. Experimental results have been fitted with two parallel RC equivalent circuits in series.

1. Introduction

Spinel ferrites are an important class of magnetic materials, which have attracted a lot of attention of scientific community because of their excellent combination of good electrical and magnetic properties [1]. In general, the cation distribution in spinel lattice has the form: $(D_{1-x}M_x)[D_xM_{2-x}]O^{-2}{}_4$, where D and M are divalent and trivalent ions respectively, and x is called the degree of inversion. The round and square brackets denote the cations located at the center of tetrahedral lattice of oxygen (A) and those at octahedral (B) lattice respectively. The high electrical resistivity and consequently low eddy currents and dielectric losses make them very important material for technological and industrial applications. These materials have wide range of applications in microwave devices, computer memories, transformers, magnetic recordings and switches [2]. The electrical properties of these materials have been the subject of continuous investigation, which depend upon the preparation conditions, amount of doping element and preparation time etc.

It is well known that impedance spectroscopy is an important method to study the electrical properties of ferrites, since impedance of the grains can be separated from other impedance sources, such as impedance of electrodes and grain boundaries. One of the important factors, which influences the impedance properties of ferrites, is micro-structural effect. Two semi-circles are often obtained in Cole–Cole plot, when the grain boundary resistance is larger than that of grain. The distributions of relaxation times, which result in deviation from ideal semi-circles, are attributed to various factors, such as disorder in the samples, and inhomogeneity in microstructures [3–6].

Tsonos et al. [7] studied the microstructure of cement mortars through dielectric parameters variation by using the complex impedance spectroscopy technique. They reported that the impedance analysis of the prepared samples revealed the existence of two short range relaxation mechanisms of conductivity. They suggested that the low frequency relaxation is related to the closed capillary pores and the high frequency relaxation to the C–S–H gel pores. Nobre et al. [8] studied the electrical properties of the $Zn_7Sb_2O_{12}$ using impedance spectroscopy. They reported that the bulk resistance curve of Zn antimoniate as a function of temperature, exhibits thermostat behaviour with negative temperature coefficient. In addition, the bulk conductivity follows the Arrhenius law with two linear branches of different slopes positioned around a region of transition temperature.

There are many studies on the impedance properties of different ferrite materials reported in the literature. Amador et al. [9] studied the effect of grain size distribution on Cole–Cole plots of Ni–Zn ferrites. They reported that the decrease in resistivity occurs with increasing grain size. They also reported that as the width of grain size distribution increases, the semi-circles exhibit a deformation and become unresolved. Sivakumar et al. [10] reported the electrical and magnetic properties of the chemically derived nanocrystalline Co ferrite. They reported that due to the smaller grain size of prepared samples (Co ferrite), the conduction mech-

* Corresponding author. Tel.: +91 9897810509; fax: +91 571 2700042.
E-mail address: khalid.mujasam@gmail.com (K.M. Batoo).

0925-8388/$ – see front matter © 2009 Elsevier B.V. All rights reserved.
doi:10.1016/j.jallcom.2009.01.137

anism takes place predominantly through the grain boundary and hence a single semi-circle is observed in the complex impedance plot. Similar results have been reported by us in our earlier paper [11], where we have reported that the impedance of grain boundary has increased with Al doping. we have also reported in Cd doped $CoFe_2O_4$ materials [12], that capacitive and resistive properties of the materials decreased up to 20% of Cd doping, and thereafter, these properties increased with further Cd doping. Bo Wang et al. [13] use the impedance spectroscopy technique to study the micro-structural dielectric constant of copper-substituted Ni–Zn ferrites. They reported that the small liquid-like particles were found filling the grain boundaries of prepared samples, which have lower dielectric constant and dielectric loss. Ponpandian et al. [14] studied the electrical conductivity and dielectric behaviour of nanocrystalline $NiFe_2O_4$ spinel. They reported that the samples with smaller grain size show only one semi-circle corresponding to grain boundary conduction, while samples of larger size show two semi-circles corresponding to both grain and grain boundary conduction mechanism. Ahmed et al. [15] studied the effect of cation concentration on the relaxation phenomena of Co–Zn ferrites. They reported that the maximum of the relaxation time (τ), calculated from the Cole–Cole plots corresponds to the critical concentration, $x = 0.6$.

In the present work, the electrical properties of Al doped $MnFe_2O_4$ ferrites have been investigated by impedance spectroscopy. It is preferable to plot the complex impedance or conductivity for characterizing our ferrite materials when dealing with charge carrier systems. The impedance spectroscopy or ac conductivity technique enables us to evaluate and separate out the contributions to overall electrical properties due to various components such as grain, and grain boundary or polarization phenomenon in a material, in the frequency or time domains. Here, the principle of analysis is based on the fact that ac response of a sample to sinusoidal electrical signal, and subsequent calculation of the resulting transfer (impedance) with respect to the frequency of the applied signal. The aim of this work is to study the bulk and interface phenomena over a wide range of frequencies and at selected temperatures in order to get information about the relaxation times, and relaxation amplitudes of various processes present in the system, when a small perturbation signal is sent to the system over a wide range of frequencies. It is worth to note that various physical parameters and characteristic properties that influence the performance of a ferrite material can be obtained from the analysis of complex impedance spectra.

2. Experimental

Polycrystalline spinel ferrites with chemical formula $MnFe_{2-2x}Al_{2x}O_4$ ($0 \le x \le 0.5$) were prepared by conventional solid state reaction technique. High purity 'AR' grade oxides, iron oxide (Fe_2O_3), aluminum oxide (Al_2O_3) and manganese oxide (MnO_2) were mixed together according to their chemical weights. The mixture of each composition was ground to a very fine powder, and calcinated at 1273 K for 12 h. The pre-calcinated powders were again ground and sintered at 1523 K for 24 h. Finally, the samples were ground to fine powder, pressed into disk shaped pellets, and sintered at 1573 K for 24 h. At the end of each heat treatment the samples were allowed to cool slowly to room temperature at a rate of 274 K/min [16]. Silver paste coating was applied on the opposite faces of pellets, in order to make parallel plate capacitor geometry and the ferrite material as dielectric medium. The complex impedance measurements were carried out using the LCR HI-Tester (HIOKI 3532-50) as a function of frequency (42 Hz to 5 MHz), and temperature (300 K–473 K).

3. Result and discussion

3.1. X-ray analysis

Fig. 1 shows the X-ray diffraction (XRD) pattern of $MnFe_{2-2x}Al_xO_4$ ($0 \le x \le 0.5$) ferrites. The XRD patterns analyzed using Powder-X software indicates that all the compositions exhibit single phase cubic spinel structure with *Fd3m* space group. The lattice parameter has been found to decrease with Al doping. The decrease in lattice parameter with x can be explained on the basis of Vegard's law [17]. The Vegard's law predicts linear change in the lattice parameter for the spinel system with the substitution of different ions. The law is based on the change due to ionic radii of replacing and replaced ions. In the present case, Al^{3+} is having smaller ionic radius (0.051 nm) compared to the radius of Fe^{3+} ion (0.064 nm).

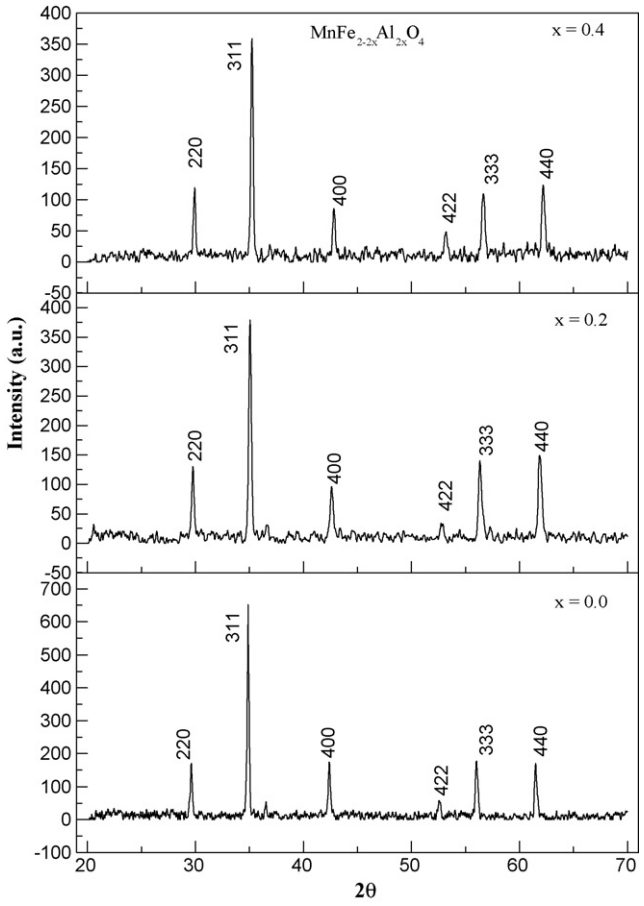

Fig. 1. XRD pattern of the $MnFe_{2-x}Al_xO_4$ ferrites.

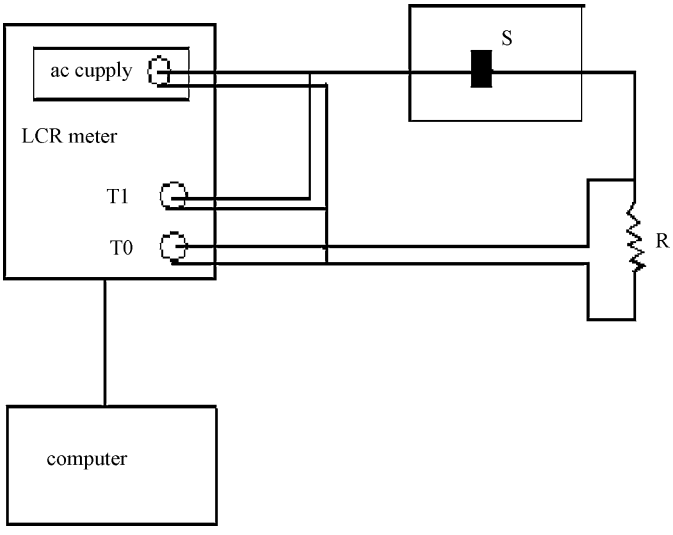

Fig. 2. Schematic diagram of the LCR meter.

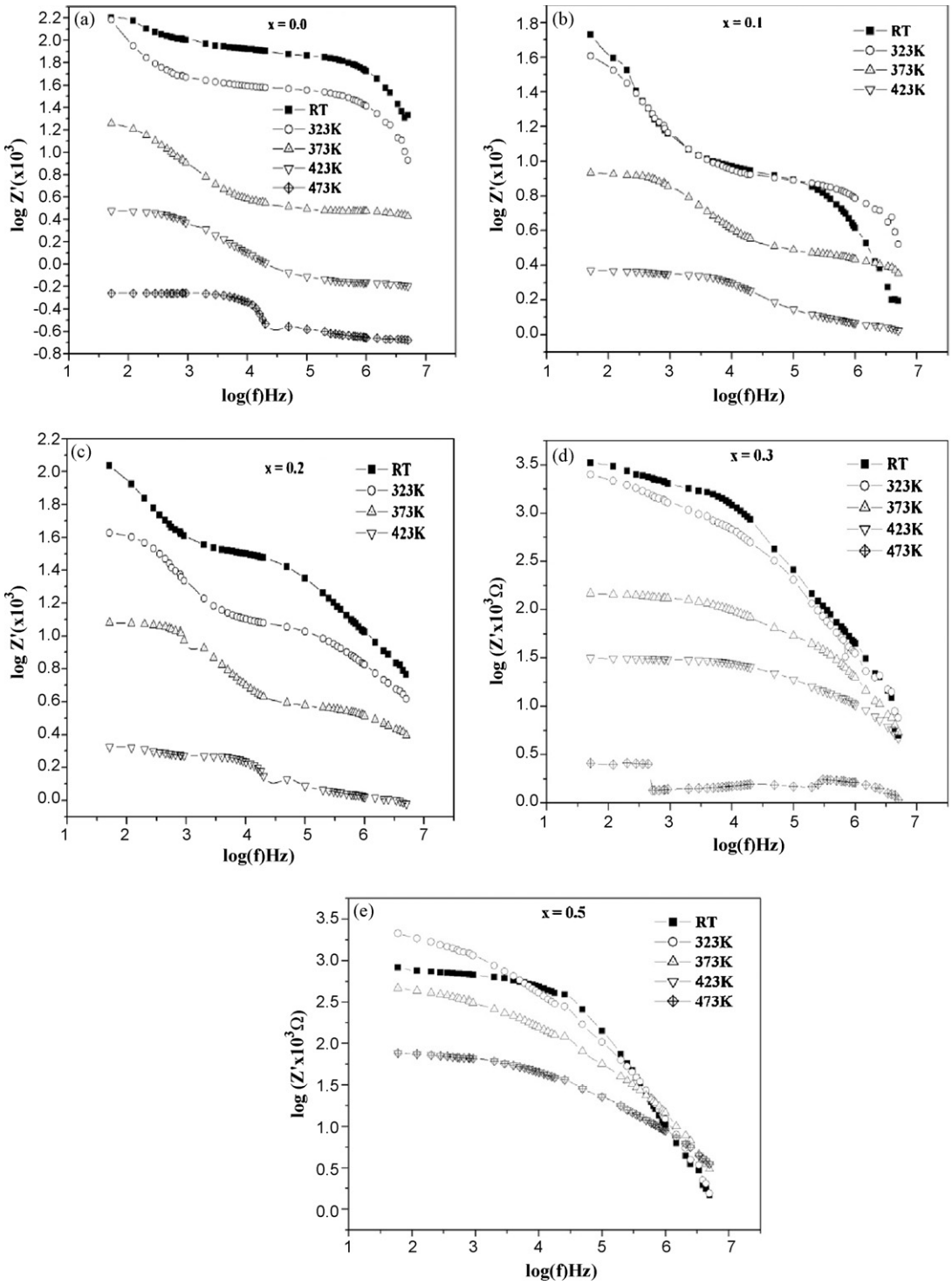

Fig. 3. Variation of real part of impedance with frequency at different temperatures.

Thus substitution of Al^{3+} ions results in a linear decrease in the lattice parameter.

3.2. Impedance spectroscopy

The real and imaginary part of the complex impedance: $Z^* = Z' - Z''$ ($j = \sqrt{-1}$) of a series of $MnFe_{2-2x}Al_{2x}O_4$ ($0 \le x \le 0.5$) ferrites have been studied as a function of frequency between 42 Hz and 5 MHz and temperature between 300 and 473 K. Fig. 2 shows the schematic diagram of the LCR circuit used for complex impedance analysis. A sine wave signal was fed to the input terminal (T_1) of the LCR meter and the sample from the signal generator (SG) terminal. The output (T_0) measured the output signal from the sample, which was voltage drop across a standard resistance of 1 kΩ. LCR then automatically analyzed the signals from T_1 and T_0 to give the phase difference (θ) between the input and out signals, i.e., Z' and Z''. The complex impedance plot is obtained after plotting Z'' versus Z'. When ac voltage $V = V_0 e^{j\omega t}$ is applied across the sample, the current that flows across the sample is given by:

$$i = j\omega CV = \frac{j\omega(\varepsilon'_r - j\varepsilon'_r)A\varepsilon_0 V}{d} \quad (1)$$

where C is the capacitance of the parallel plate capacitor with the ferrite material as the dielectric and ε_0 is permittivity of free space.

Fig. 3(a)–(e) shows the variation of real part of impedance (Z') with frequency at selected temperatures for various compositions. It is clearly seen that the Z' decreases with increasing frequency. The decrease in the value of Z' with increasing frequency shows that the conductivity of the Mn ferrites increases as the frequency increases. The conductivity of the samples also increases with increasing temperature, which shows that the ferrite materials exhibit semiconductor nature.

Fig. 4(a)–(e) shows the variation of resistive (imaginary) part of impedance (Z'') as a function of frequency at selected temperatures for various different compositions. It is seen that Z'' decreases with increasing frequency but increases with increasing temperature. All plots of Z'' versus frequency at various temperatures for the different compositions exhibit broad Debye peaks, which show the existence of relaxation processes in these materials. These peaks are

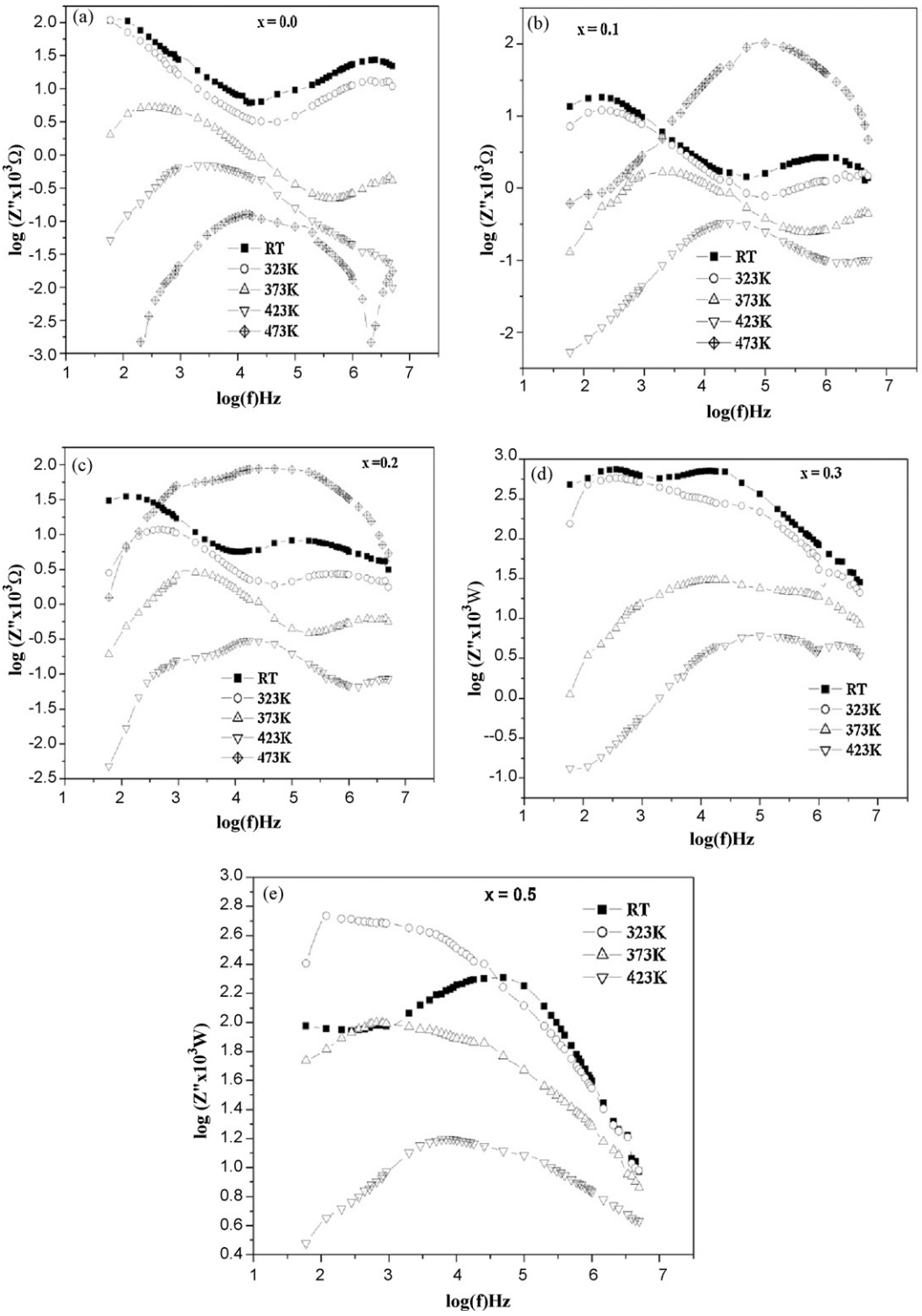

Fig. 4. Variation of imaginary part of impedance with frequency at different temperatures.

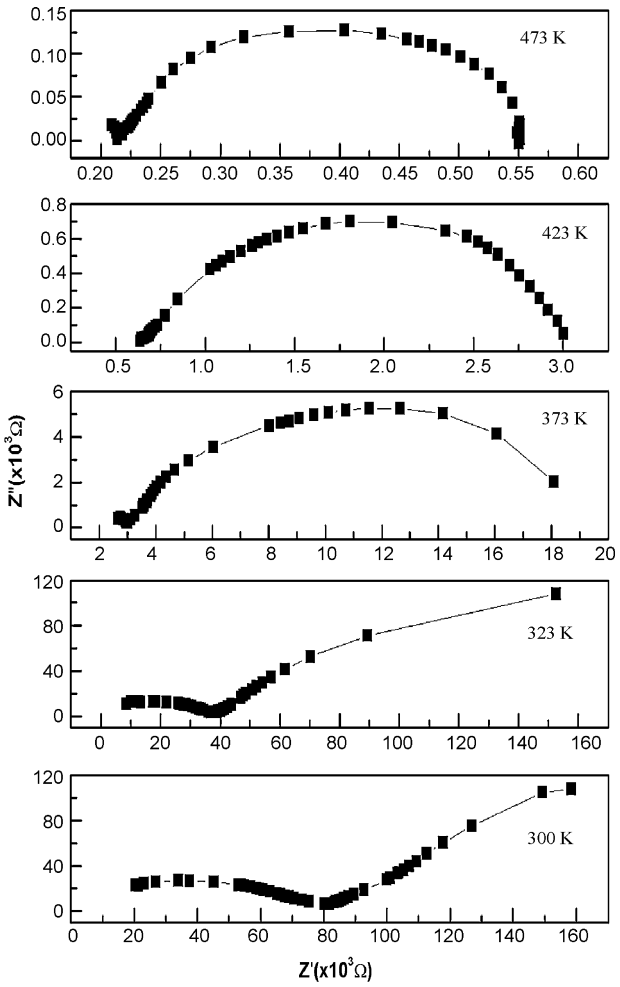

Fig. 5. Complex impedance for the composition $x = 0.0$, at selected temperatures.

shifted towards higher temperature by increasing frequency from 42 Hz to 5 MHz. There are three generic relaxation dispersion situations, which may occur for solids while discussing Z' as a function of frequency: conductive system associated charge carriers, dielectric dispersion usually arising from dipole rotation of lattice entities and the presence of both types of dispersion within measured frequency range. Three different dipolar relaxation processes and an intrinsic conductivity contribution may be involved in this case [18]. The value of Z'' maxima decreases with temperature for all the compositions, which indicate the increasing loss in the resistive property of the sample. Such behaviour is expected due to the presence of space charge polarization in the materials [19]. The occurrence of relaxation peaks in the real and imaginary part of complex impedance at low frequencies with temperature may be due to the existence of the space–charge relaxation at low frequencies, which is related to the charge carriers in association with the oxygen vacancies. The conductivity is dominated by the short range hopping of charge carriers at low temperature. In order to form space charge polarization, few oxygen vacancies are trapped at the electrode interface, which are due to the high mobility of oxygen vacancies in the Al doped Mn ferrites, where they can move easily, when externally applied electric field is turned on, resulting in a little space charge effect at low temperatures. In contrast, at high temperatures, more oxygen defects are activated, and they are accumulated at the electrode interfaces and grain boundaries resulting in a strong space charge relaxation [20,21].

The impedance spectroscopy helps in the separation of grain and grain boundary because each of them has different relaxation times,

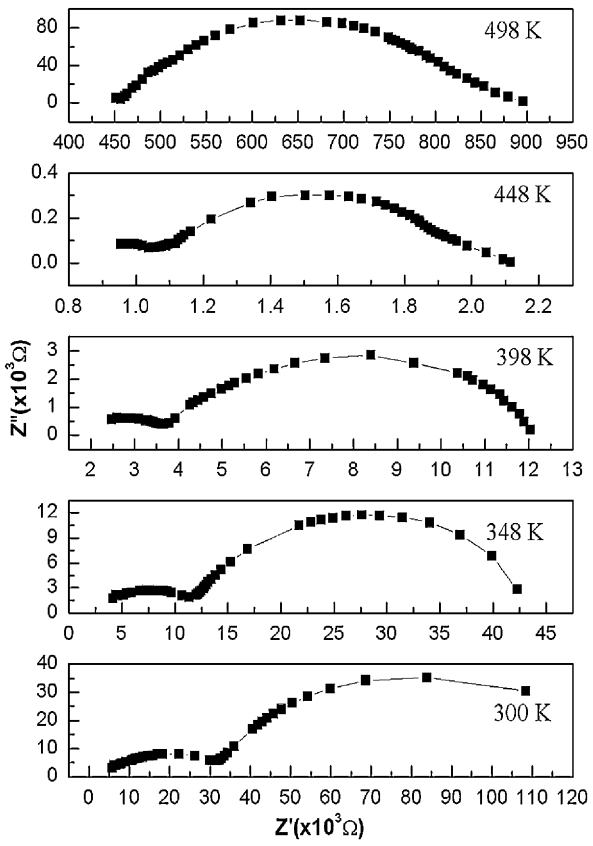

Fig. 6. Complex impedance for the composition $x = 0.2$, at selected temperatures.

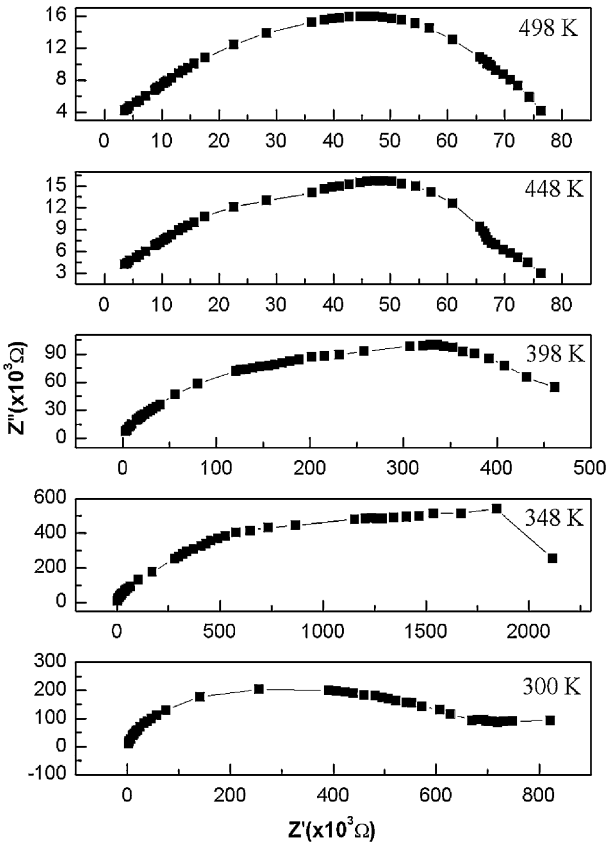

Fig. 7. Complex impedance for the composition $x = 0.4$, at selected temperatures.

Table 1
Impedance parameters calculated from the complex impedance plots for various compositions at different temperatures.

Chemical formula	R_g (kΩ)	C_g (F)	τ_g (s)	R_{gb} (kΩ)	C_{gb} (F)	τ_{gb} (s)
T = 300						
$MnFe_2O_4$	–	–	–	78.171	4.69E-7	0.036
$MnFe_{2.3}Al_{0.2}O_4$	–	–	0.055	6.7054	5.6E-5	0.376
$MnFe_{2.1}Al_{0.4}O_4$	77.24	3.66E-7	0.028	25.374	4.84E-6	0.123
$MnFe_{1.7}Al_{0.8}O_4$	–	–	–	564.41	1.12E-9	1.77E-3
$MnFe_{1.5}Al_1O_4$	–	–	–	819.82	4.85E-3	5.92E-9
T = 348 K						
$MnFe_2O_4$	–	–	0.009	34.922	2.03E-6	0.0707
$MnFe_{2.3}Al_{0.2}O_4$	32.69	2.52E-6	0.0826	4.288	1.53E-4	0.656
$MnFe_{2.1}Al_{0.4}O_4$	30.951	2.7E-6	0.0849	7.19	5.1E-5	0.3668
$MnFe_{1.7}Al_{0.8}O_4$	–	–	–	843.34	4.25E-9	3.58E-3
$MnFe_{1.5}Al_1O_4$	–	–	–	2113.24	8.96E-10	1.89E-3
T = 398 K						
$MnFe_2O_4$	13.428	1.4E-5	0.1898	0.9081	2.35E-3	2.132
$MnFe_{2.3}Al_{0.2}O_4$	5.7	2.52E-6	0.0826	4.288	32.69	0.656
$MnFe_{2.1}Al_{0.4}O_4$	8.369	0.352	4.21E-5	1.191	1.56E-3	1.865
$MnFe_{1.7}Al_{0.8}O_4$	–	–	–	44.458	1.79E-6	0.0799
$MnFe_{1.5}Al_1O_4$	–	–	–	459.12	2.163E-8	9.93E-3
T = 448 K						
$MnFe_2O_4$	–	–	–	2.375	6.03E-4	1.432
$MnFe_{2.3}Al_{0.2}O_4$	1.213	2.49E-3	3.021	0.081	0.122	9.775
$MnFe_{2.1}Al_{0.4}O_4$	1.0781	3.075E-3	3.315	0.0838	0.139	3.315
$MnFe_{1.7}Al_{0.8}O_4$	–	–	–	6.494	7.08E-5	0.459
$MnFe_{1.5}Al_1O_4$	–	–	–	72.81	8.59E-7	0.063
T = 473 K						
$MnFe_2O_4$	0.3361	2.34E-2	7.88	0.016	3.496	55.55
$MnFe_{2.3}Al_{0.2}O_4$	–	–	–	280.2	3.47E-8	9.7E-3
$MnFe_{2.1}Al_{0.4}O_4$	–	–	–	444.48	2.55E-8	0.0113
$MnFe_{1.7}Al_{0.8}O_4$	–	–	–	0.706	5.06E-3	3.572
$MnFe_{1.5}Al_1O_4$	–	–	–	72.8	8.44E-7	6.15E-2

resulting in separate semi-circles in complex impedance plane. The spectrum reveals relatively large grain boundary contribution to the total resistivity because close to the grain boundaries, transport properties of the materials are controlled by imperfections, expected to be present in higher concentration than in grains, leading to an additional contribution to the inter-grain (grain boundary) impedance. The internal space charge created at the grain boundaries may lead to a significant increase in the concentration of mobile effects [22]. The complex impedance plot can be represented in terms of any of the five possible complex formalisms, the permittivity (ε^*), the admittance (Y^*), the electric modulus (M^*), the impedance (Z^*) and the loss tangent ($\tan\delta$). These parameters are related with each other [23] by the formula:

$$\tan\delta = \frac{\varepsilon''}{\varepsilon'} = \frac{M''}{M'} = \frac{Y''}{Y'} = \frac{Z''}{Z'} \tag{2}$$

whereas the real and imaginary parts of the complex impedance are given by

$$Z' = \frac{R_g}{(1+\omega_g C_g R_g)^2} + \frac{R_{gb}}{(1+\omega_{gb} C_{gb} R_{gb})^2} \tag{3}$$

and

$$Z'' = \frac{-R_g^2 \omega_g C_g}{1+(R_g \omega_g C_g)^2} + \frac{-R_{gb}^2 \omega_{gb} C_{gb}}{1+(R_{gb} \omega_{gb} C_{gb})^2} \tag{4}$$

where the terms R_g and C_g represents the resistance and capacitance of the grain, while R_{gb} and C_{gb} represents the corresponding terms for the grain boundary volume [24]. The resistance value for the grain and grain boundary has been calculated from the intercepts on the real part of Z (Z') axis, where as the capacitance values have been calculated from the frequency peaks of the semi-circle arcs. Since the value of $Z' = -Z''$ at the maximum, we have;

$$C_g = \frac{1}{R_g \omega_g} \tag{5}$$

$$C_{gb} = \frac{1}{R_{gb} \omega_{gb}} \tag{6}$$

Also, the relaxation times τ_g and τ_{gb} have been calculated from the frequency peaks using the equations:

$$\tau_g = \frac{1}{\omega_g} = C_g R_g \tag{7}$$

$$\tau_{gb} = \frac{1}{\omega_{gb}} = C_{gb} R_{gb} \tag{8}$$

The peak frequency for grain boundaries is much smaller than that for grains due to their large resistance and capacitance compared to those of grains [25]. Due to this fact we attribute the higher frequency response, which corresponds to the small arc (see Figs. 5 and 6) to the grains and the lower one to the grain boundaries. The resistance of the grain boundary is larger than that of the grain, i.e., $R_{gb} \geq R_g$.

The complex impedance plots or Cole–Cole plots for the various compositions of Mn ferrites as a function of frequency at different temperatures (300–473 K) are shown in Figs. 5–7. It is seen that the two semi-circles are observed for the compositions, x = 0.0 and 0.2 at low temperature, while only one semi-circle is observed at 473 K, which shows the predominance of the grain boundary resistance at the 473 K. For compositions, x = 0.0, 0.4 and 0.5 only one semi-circle has been observed at low as well as at high temperatures, which shows the predominating influence of grain boundary impedance in these compositions. It is seen that there are two effects pertaining to the micro-structural inhomogeneity—grain and grain boundary. No other relaxation mechanism, such as the electrode effect and ionic species diffusion, is identified for the analyzed frequency range.

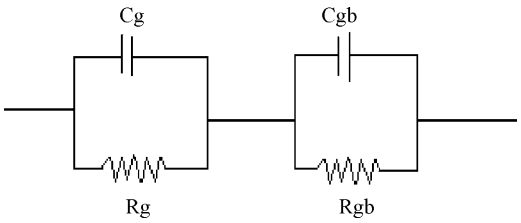

Fig. 8. Proposed circuit for the analysis of impedance spectroscopy data.

Different electrical parameters calculated from the complex impedance plots for the various compositions at selected temperatures are shown in Table 1. It is observed that the grain boundary resistance decreases up to 448 K, thereafter it increases with further increasing the temperature. The capacitance of grain boundary is found to increase with increasing temperature, which means the polarizability increases with the increasing temperature. For all the samples the capacitance of the grain boundary (C_{gb}) is higher than that of the grain (C_g), which is explained on the basis that the capacitance is inversely proportional to the thickness of the media. The value of C_g and C_{gb} are found to be maximum, which means Al doped Mn ferrites are having greater polarizability. The lower value of total resistance R_g and R_{gb} for the composition, $x = 0.2$, indicates that the phenomena of electron hopping mechanism is promoted in this composition, which is a sole mechanism for the process of conduction and polarizability. The value of the grain boundary resistance is found to be larger than the resistance of the grain, in addition, the semi-circle arc is found distorted at higher temperature, which is attributed to the fact that the atomic arrangement at the grain boundary is disordered, giving enhancement in electron scattering process. The higher value of grain boundary impedance can be because of the fact that the Fe^{2+} ion species decrease in the region [26].

For the analysis of the experimental results, it is assumed that the material consists of piled up crystalline plates, as a microstructure formed by parallel conducting plates (grains) separated by resistive plate boundaries (grain boundaries). Therefore, the imaginary part of the impedance (Z'') is plotted against the real part of the impedance (Z'). Two semi-circles are obtained. Each semi-circle arc corresponds to resister–capacitor RC phase. The semi-circle at low frequency side corresponds to the grain boundary, while the semi-circle at higher frequency side corresponds to the grain. Such an interpretation is indeed very helpful to represent the sample by an electrical circuit as a combination of resistors and capacitors as shown in Fig. 8, and analytically explained by Eqs. (3) and (4). Such interpretations have also been given earlier [27–29] for amorphous chalcogenides. The representation of sample through an electrical analog circuit is very helpful in representing the electrical features of the sample [26]. In this circuit, a resistance represents a conductive path and a given resistor in a circuit might account for the bulk conductivity of the sample. Also the capacitances will be generally associated with space charge polarization regions.

4. Conclusion

We have successfully synthesized single phase polycrystalline $MnFe_{2-2x}Al_{2x}O_4$, using solid state reaction technique. The real and imaginary parts of the impedance have been found to decrease by increasing the temperature, which shows the conductivity of Mn ferrite increases with the temperature, confirming the semiconductor behaviour of the system. Two semi-circles have been observed for the compositions, $x = 0.1$ and 0.2 at low temperature, while only one semi-circle has been observed at 473 K, which shows the predominance of the grain boundary resistance at 473 K. For compositions, $x = 0.0$, 0.4 and 0.5 only one semi-circle has been observed at low as well as at high temperature, which is due to the large contribution by the grain boundaries in these compositions. The values of R_g and R_{gb} are minimum for the composition, $x = 0.2$, which shows that the ac conductivity of the composition is very high. The analysis of the complex impedance data shows that the capacitive and reactive properties of the materials are mainly attributed due to the processes which are associated with the grain and grain boundary.

Acknowledgements

One of the authors K.M. Batoo is thankful to I.U.A.C, New Delhi, India, for financial support though UFUP project. Authors S.K. and C.G. Lee acknowledge Korea Research Foundation (Grant KRF-2008-005-J02703) for the financial support.

References

[1] N.S. Gajbhiye, G. Balaji, S. Bhattacharyya, M. Ghafari, Hyp. Int. 156/157 (2004) 57.
[2] J. Smith, H.P.J. Winjin, Ferrites, Philips, Eindhoven, 1959.
[3] J.T.S. Irvine, D.C. Sinclair, A.R. West, Adv. Mater. 3 (2004) 132–138.
[4] H.F. Cheng, J. Appl. Phys. 56 (1984) 1831–1837.
[5] S.C. Byeon, K.S. Hong, J.G. Park, W.N. Kang, J. Appl. Phys. 81 (1997) 7835–7841.
[6] D. Arcos, M. Vazquer, R. Valezuela, M. Vallet-Regi, J. Mater. Res. 14 (1999) 861–865.
[7] C. Tsonos, I. Stavrakas, C. Anastasiadis, A. Kyriazopoulos, A. Kanapitsas, D. Triantis, J. Phys. Chem. Sol., doi:10.1016/j.jpcs.2008.12.015.
[8] M.A. dE Lima Nobre, S. Lanfredi, J. Mater. Res. 2 (2003) 151–155.
[9] M.P. Gutierrez-Amador, R. Valenzuela, Mater. Res. Soc. Symp. Proc. (2002) 699.
[10] N. SivaKumar, A. Narayanasamy, K. Shinoda, C.N. Chinnasamy, B. Jeyadevan, J.M. Greneche, J. Appl. Phys. 102 (2007) 013916.
[11] K.M. Batoo, et al., Curr. Appl. Phys. (2008), doi:10.1016/j.cap.2008.08.001.
[12] A.M.M. Farea, S. Kumar, K.M. Batoo, A. Yousef, C.G. Lee, Alimuddin, J. Alloys Compd. 464 (2008) 361–369.
[13] H. Bo Wang, J.H. Liu, W.F. Li, J. Bo Wang, L. Wang, L.J. Song, S.J. Yuan, F.S. Li, J. Alloys Compd. 461 (2008) 373–377.
[14] N. Ponpandian, P. Balaya, A. Narayanasamy, J. Phys. Cond. Mater 14 (2002) 3221–3237.
[15] M.A. Ahmed, K.A. Darwish, H. Mikhail, M. Mounir, E.H. El-khawas, Phys. Scripta (1997) 750–755.
[16] S. Kumar, R. Kumar, S.K. Sharma, V.R. Reddy, A. Benerjee, Alimuddin, Solid. Stat. Comm. 12 (2007) 706–709.
[17] C.G. Whinfrey, D.W. Eckort, A. Tauber, J. Am. Chem. Soc. 82 (1960) 2695.
[18] S. Dutta, R.N.P. Choudhary, P.K. Sinha, Phys. Stat. Sol. (a) 202 (2005) 1172–1181.
[19] H. Groothues, F. Kremer, P.G. Schouten, J.M. Warman, Adv. Mater. 7 (1995) 283.
[20] S. Dutta, P.K. Sinha, R.N. Choudhary, J. Appl. Phys. 96 (2004) 1607.
[21] I.W. Kim, C.W. Ahn., J.S. Kim, T.K. Song, J.S. Lee, Appl. Phys. Lett. 80 (2002) 4006.
[22] A.R. James, S. Balaji, S.B. Krupanidhi, Mater. Sci. Eng. B 64 (1999) 149.
[23] J.R. Macdonald, Impedance Spectroscopy, Wiley, New York, 1987.
[24] G.S. Surravanshi, C.N. Jadhav, S.A. Patil, S.R. Sawan, J. Less-Comm. Meter. (1991) 168–169.
[25] D. Arcos, M. Vazqez, R. Valenzuela, M. Vallet-Regi, J. Mater. Res. 3 (1999) 861.
[26] A.K. Joncher, Relaxations in Solids, Chelsa dielectric Press, London, 1983.
[27] S. Gautam, N. Goyal, J. Ovon. Res. (2007) 111–118.
[28] S. Gautam, A. Thakur, S.K. Tripathi, N. Goyal, J. Non-Cryst. Solids 353 (2007) 1315–1321.
[29] R. Rizwan, T.R. Krishna, A.R. James, P. Sarah, Cryst. Res. Technol. 42 (2007) 699–706.